Chapter 2

Band Structure and Optical Properties

The band structure of semiconductors is mainly influenced by the lattice type, the bonding distance, and the ionicity of bonding partners. Have a look along the group IV element column of the periodic table, and one will find a thermodynamically stable diamond (zincblende) lattice type for silicon and a zincblende lattice type for AlP. The diamond (zincblende) lattice can be described by a cubic cell with eight atom positions, where all the positions are occupied by one element, A, (diamond lattice) or by two elements, A and B, from group III and group V elements, respectively. The lattice is strongly bonded by covalent forces between an atom and its immediate four neighbors (diamond lattice) and additionally by ionic forces in the zincblende lattice. The A (111) stacking of planes in the zincblende lattice may be described by an (abc) sequence a, b, c, a, b, c, ... This lattice scheme is only challenged at the low atomic number Z end (carbon, $Z = 6$; SiC, $Z = 10$) and at the high atomic number end (tin, $Z = 50$). For carbon the diamond lattice is metastable whereas the stable lattice is the layered graphite structure. A single or a few layers of graphite are now in research focus as graphene that can be considered as a narrow graphite quantum well. On the tin side the semiconducting α-Sn (gray tin) is only stable below 17°C; above room temperature the metallic β-Sn is stable. Alloying of Sn with small amounts of Ge stabilizes the diamond structure. Increasing ionicity by choosing atomic partners from group II (A) and group VI (B) favors a different lattice cell (hexagonal wurtzite lattice) that has

Silicon-Based Photonics
Erich Kasper and Jinzhong Yu

ISBN 978-981-4303-24-8 (Hardcover), 978-1-315-15651-4 (eBook)
www.jennystanford.com

the same nearest-neighbor bonding as the zincblende lattice but a different stacking in the next nearest (111) plane. The (111) stacking in the hexagonal wurtzite lattice has an (ab) sequence with a, b, a, b, ... A wrong sequence is called a stacking fault, in the sense that the wurtzite lattice is considered as a zincblende lattice with a periodic stacking fault arrangement. A special situation is given with silicon carbide (SiC) where the stacking fault energy is very low, allowing a variety of (111) arrangements (polytypic SiC) from zincblende to wurtzite, with stacking faults of decreasing periods. The diamond lattice SiC is named "cubic-SiC" or "β-SiC."

2.1 Bonding Lengths in a Diamond/Zincblende Lattice

To simplify the discussion we concentrate now on the majority of applications with diamond (zincblende) lattices. The lattice constant a_0 increases with an increasing atomic number Z (mean number $Z = 1/2(Z_A + Z_B)$ for AB compounds). In Table 2.1 a comparison of group IV and group III/V elements/compounds is given. The lattice constant a_0 [1] and the normalized lattice constant $a_0/Z^{1/3}$ are shown in picometers (1 pm = 10^{-12} m). The atomic diameter increases roughly with $Z^{1/3}$.

The bonding length, that is the lattice constant a_0, determines largely the bandgap, with sharply decreasing gaps as the lattice constant increases. The bonding length is given as $a_0 \cdot \sqrt{3}/4$. The direct bandgap that separates the valence band maximum (which is always at the Brillouin zone center, wave vector $k = 0$, named Γ) from the lowest conduction band at Γ is given as E_{gdir}. From C to SiC to Si to Ge to Sn it reduces from 6.5 eV to 6 eV to 3.2 eV to 0.8 eV to 0 eV, spanning the transition from a semi-insulator to a semimetal.

In many semiconductors of this group the lowest bandgap is indirect, which means the lowest conduction band is either in (111) direction (called L point) or in (100) direction (Δ point; the final (100) in the Brillouin zone is named the X point). The indirect transition needs a phonon help to fulfil the momentum conservation. Absorption and photon emission are much weaker in indirect transitions than in direct transitions. In Fig. 2.1 the indirect bandgaps are named E_{gL} (Γ valence band to L conduction band transition) or E_{gx} (Γ valence band to X or Δ conduction band

transition). The L conduction band energies decrease rapidly, with bond length dominating the indirect bandgap material Ge, whereas the indirect semiconductors C and Si are characterized by a Δ (E_{gx}) conduction band minimum.

Table 2.1 Cubic diamond/zincblende lattice

Element/ compound	Atomic number Z	Lattice constant a_0 (pm)	Normalized lattice constant $a_0/Z^{1/3}$ (pm)
C (diamond)	6	356.7	196.3
BN	6	361.15	198.7
SiC	10	436	202.4
AlN	10	438	203.3
Si	14	543.1	225.3
AlP	14	546.7	226.8
Ge	32	564.6	177.8
GaAs	32	565.3	178.1
Sn	50	648.9	176.1
InSb	50	648	175.9

Note: Given are the lattice constant a_0 and the normalized lattice constant $a_0/Z^{1/3}$ (Z means atomic number) as a function of Z.

Table 2.2 Bandgaps E_{gdir}, E_{gL}, and E_{gx} of group IV elements and their III/V counterparts with the same mean atomic number Z

Element	Lattice type	Z	E_{gdir} (eV)	E_{gL} (eV)	E_{gx} (eV)
α-Sn	D	50	−0.41	0.14	0.9
InSb	ZB	50	0.25	1.08	1.71
Ge	D	32	0.8	0.66	0.85
GaAs	ZB	32	1.42	1.25	1.94
Si	D	14	3.2	1.65	1.12
AlP	ZB	14	3.62	—	2.49
SiC	ZB	10	6	4.2	2.2
AlN	ZB	10	6.2	—	—
C	D	6	6.5	9.2	5.45
BN	ZB	6	8.2	—	6.4

Note: The lattice type is diamond (D) or zincblende (ZB). Direct semiconductors are underlined, and the lowest transition is underlined.

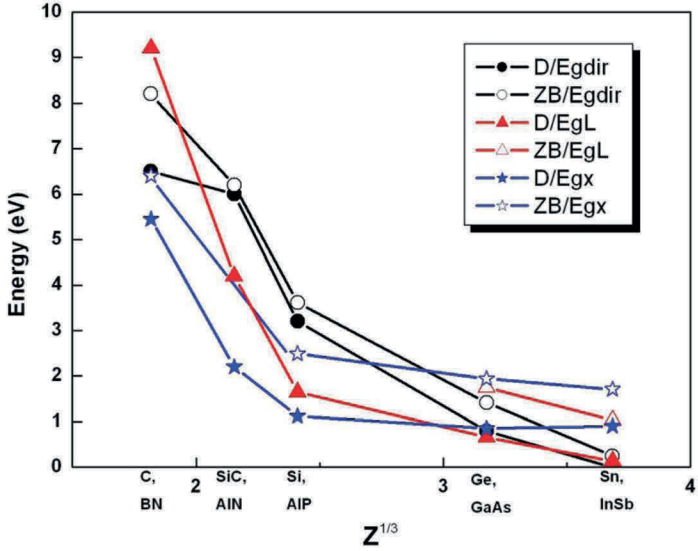

Figure 2.1 Band edge energies for different group VI and group III/V compounds as a function of $Z^{1/3}$ (Z means atomic number). Group IV is given by full symbols and group III/V by empty ones. E_g is black, E_{gL} red, and E_{gx} blue.

Compare group VI with group III/V materials to identify the influence of the ionicity that contributes to group III/V compounds. At all energy levels—direct and indirect, L or X—the ionicity increases the transition energies and strengthens the tendency for direct semiconductors; see AlN, GaAs, and InSb (Table 2.2) compared to Si, Ge, and Sn.

2.2 Dielectric Function

The macroscopic influence of a material on the electrical properties is described by a complex dielectric function $\underline{\varepsilon}_r$ [2],

$$\underline{\varepsilon}_r = \varepsilon_r' + j\varepsilon_r'' , \tag{2.1}$$

that links the electric field strength $\vec{E}$ with the electric displacement vector $\vec{D}$ by the well-known relation

$$\vec{D} = \underline{\varepsilon}_r \varepsilon_0 \cdot \vec{E} . \tag{2.2}$$

For static fields or low-frequency modulation the displacement vector is in phase with the electric field and then the dielectric

function reduces to the dielectric constant (permittivity) ε_r. For a higher circular frequency the dielectric displacement is out of phase, which is described by the complex dielectric function $\underline{\varepsilon}_r$. Figure 2.2 shows the dielectric function of silicon at room temperature in the spectral range of interband transitions as obtained by spectroscopic ellipsometry [3]. The dominant contribution to the frequency dependence of the dielectric function of semiconductors arises from electronic interband transitions between occupied valence band and empty conduction band states. Conservation of momentum imposes direct transitions without a change of wave vector for a first-order process.

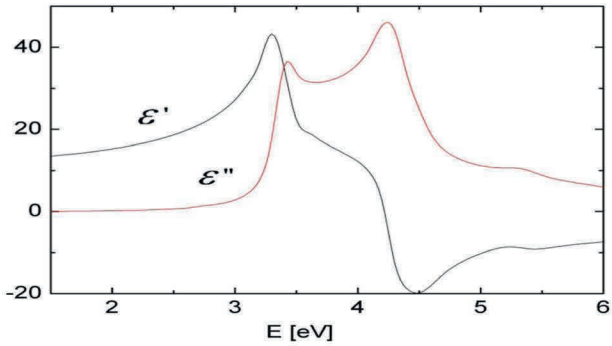

Figure 2.2 Dielectric function $\underline{\varepsilon} = \varepsilon' + j\varepsilon''$ of silicon versus photon energy.

The phase delay is explained by atomistic theories that take into account the polarization $\vec{P}$ of a material under the influence of an electrical field. One can immediately imagine that an atom is polarized by the different forces on the positive nucleus charge and the negative electron cloud charge or that in an ionic crystal an additional term is created by the different charges on the crystal lattice sites. The originally classical mechanics and later quantum mechanical theories of polarization $\vec{P}$ are the base of a quantitative understanding of the dielectric function of different dielectrics and semiconductors,

$$\vec{D} = \varepsilon_0 \cdot \vec{E} + \vec{P} \tag{2.3}$$

From Eqs. 2.2 and 2.3

$$\vec{P} = \varepsilon_0 (\underline{\varepsilon}_r - 1) \cdot \vec{E} \,. \tag{2.4}$$

The linear polarization property ($\varepsilon_r - 1$) is termed electrical susceptibility χ:

$$\chi = \varepsilon_r - 1 \tag{2.5}$$

For the description of an electromagnetic wave in a nonmagnetic material a related set of optical constants is more practical.

Let us define a complex quantity

$$\underline{n} = (\underline{\varepsilon_r})^{1/2}, \tag{2.6}$$

which is the square root of the dielectric function.

This complex quantity n is composed of the refractive index n and the absorption index κ:

$$\underline{n} = n - j\kappa \tag{2.7}$$

This follows from the solution (Maxwell's equations) of an electromagnetic wave in a nonmagnetic semiconductor

$$E = E_0 \exp[j(wt - k_0 \underline{n} x)]. \tag{2.8}$$

The vacuum wave number k_0 is given by

$$k_0 = 2\pi/\lambda_0, \tag{2.9}$$

with λ_0 as the vacuum wavelength.

The physical meaning of n and κ will be clearer after separating the imaginary and real parts in the wave equation, Eq. 2.8.

$$E = E_0 \exp[j(wt - k_0 \underline{n} x)]\exp(-k_0 \kappa x) \tag{2.10}$$

The refractive index n describes the wave vector in a material

$$k = k_0 \cdot n \text{ or } \lambda = \lambda_0/n, \tag{2.11}$$

whereas the absorption index describes the attenuation of the field strength $\vec{E}$ on a $k_0 x$ scale.

For measurement purposes the absorption coefficient α is more convenient, which is a measure of the intensity attenuation on a pure length scale. Because the intensity is proportional to the square of the $\vec{E}$ field, this absorption coefficient reads as follows:

$$\alpha = 2k_0 \kappa \tag{2.12}$$

The relations between the optical constants n and κ and the dielectric function are summarized in the following equation:

$$\varepsilon_r' = n^2 - \kappa^2 = n^2 - (\alpha^2/4k_0^2) \tag{2.13}$$

$$\varepsilon_r'' = 2n\kappa = n\alpha/k_0 \tag{2.14}$$

The frequency dependencies of the dielectric function components ε_r' and ε_r'' are not independent; they are linked by the Kramers–Kronig relationship

$$\varepsilon_r'(\omega^*) - 1 = \frac{2}{\pi} \int_0^\infty \frac{\omega \varepsilon_r''(\omega)}{\omega^2 - (\omega^*)^2} d\omega \tag{2.15}$$

and

$$\varepsilon_r''(\omega^*) = -\frac{2\omega^*}{\pi} \int_0^\infty \frac{\varepsilon_r'(\omega) - 1}{\omega^2 - (\omega^*)^2} d\omega . \tag{2.16}$$

That means if the whole frequency dependence of one component is known the other can be calculated by a numerical integration.

2.3 Absorption Processes

In the visible and near-infrared spectral regime the fundamental absorption processes [4] can be easily explained considering the electronic band structure of semiconductors and keeping in mind the conservation laws of energy and momentum. The energy E_{ph} of a photon is rather high in this spectral range,

$$E_{ph}(\omega) = \hbar\omega = 1.24eV/\lambda_0 \ (\mu m), \tag{2.17}$$

with a rather small momentum $\vec{p}_{ph}$

$$\vec{p}_{ph}(\omega) = \hbar k_0 = \hbar\omega/c \ (\text{vacuum}) \tag{2.18}$$

compared to the momentum space $\vec{p}_{max}$ given by the first Brillouin zone

$$\vec{p}_{max} = \hbar k_{max} = \hbar\pi/a_0 \ (\text{diamond lattice}) \tag{2.19}$$

as $\vec{p}_{ph}/\vec{p}_{max} = 2a_0/\lambda_0$ is typically on the order of 10^{-3} (Si, $\lambda_0 = 1.1$ µm). The phonon energies are rather low (Si: below 65 meV), but they cover the whole momentum space. As an example Fig. 2.3 shows the energy versus wave vector diagram of transversal optical (TO) and transversal acoustic (TA) phonons in Si.

TO phonons have got energies rather insensitive to the wave number. TA phonon energies start roughly linear with wave numbers.

Interband absorption (valence band to conduction band) requires as minimum energy the bandgap transition E_g. This gives

a clear cutoff wavelength above which no interband absorption is possible.

$$\lambda_{\text{cutoff}} = 1.24\ \mu\text{m}/E_{\text{g}}\ (\text{eV}) \tag{2.20}$$

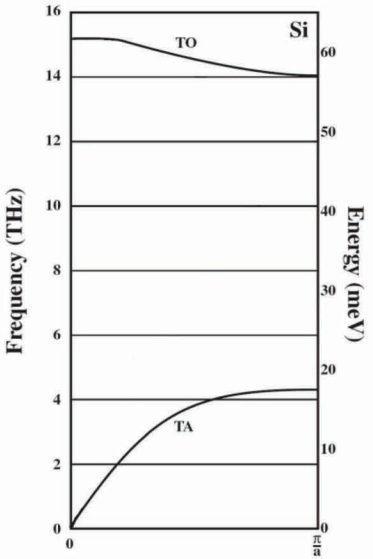

Figure 2.3 The phonon spectra along the (100) direction in Si. Shown are the transverse modes TO and TA, respectively (O: optical, A: acoustic).

Absorption above E_{g} is strongly dependent on the type of transitions (direct or indirect) because indirect transitions need phonons to satisfy momentum conservation. One obtains easy relations for the absorption coefficient, assuming effective mass approximation for the electronic band structure.

Direct transition: $\alpha \cdot \omega = A\ (E_{\text{ph}} - E_{\text{g}})^{1/2}$ (2.21)

Within a limited energy range near the band extremum (where effective mass approximation is valid for steady functions) this relation is often simplified as α^2 proportional to $(E_{\text{ph}} - E_{\text{g}})$.

Indirect transition: The onset of absorption caused by indirect transitions is much weaker due to the phonon contribution for momentum conservation. It is described by

$$\alpha = A'\ (E_{\text{ph}} - E_{\text{g}})^2 \tag{2.22}$$

The extracted bandgap E_g is in reality a temperature-dependent mixture of two curves for $E_g + E_{phon}$ and $E_g - E_{phon}$ because absorption and emission of a phonon are possible. As an example silicon absorption [5] is shown (Fig. 2.4) because Si is completely indirect in its band structure up to 3.2 eV. The square root of the absorption coefficient versus the energy scale should give a straight line for indirect semiconductors. This is fulfilled near the band edge when the effective mass model is a good description of the density of states of the bands. Photocurrent spectroscopy may be used for absorption measurements of thin layers of materials [6] in order to assess direct or indirect fundamental absorption and to estimate the band edge energy. However, near energetic distances between indirect and direct bandgap as given in pure Ge or GeSn alloys result in higher resonant indirect optical absorption [7].

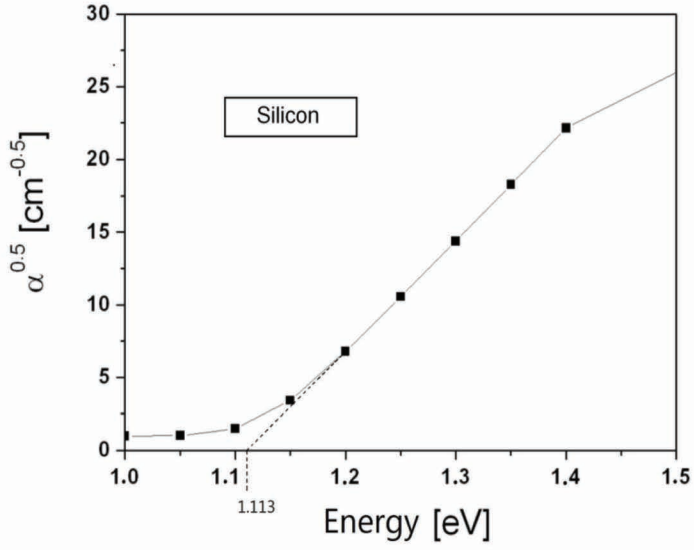

Figure 2.4 The room temperature absorption α of Si, depicted as $\alpha^{0.5}$ versus E_{ph}.

2.4 Direct Group IV Semiconductors

Unstrained alloys change their lattice cell volume V with composition. The relative volume change $\Delta V/V$ with respect to a reference

cell depends on the lattice mismatch f between the alloy and the reference. We treat the corresponding bandgap changes within a linear approximation, which delivers enough accuracy within a few percent volume change because the data for deformation potentials and indirect/direct conduction band crossover are uncertain by at least 10%.

$$\Delta V/V = 3f \tag{2.23}$$

The lattice mismatch f is $0.043*x$ for SiGe, with Si as reference, and $0.147*y$ for GeSn, with Ge as reference, respectively. The molar concentration of Ge in SiGe is given by x, and the molar concentration of Sn in GeSn is given by y.

With increasing lattice cell volume of GeSn, the energy difference ΔE_c between the direct conduction band and the indirect one shrinks from 136 meV for Ge to 0 meV for GeSn at the crossover concentration. The crossover concentration of Sn in GeSn is assessed to be between 7% and 11% [8]. The uncertainty stems from the contribution of residual strain and the low detectivity of weak indirect transitions near the strong direct transitions. The following numerical values for the linear approximation are consistent with data from Ref. [9]. In this work, the crossover is obtained either with 9% Sn in GeSn or 2% biaxial tensile strain. A linear superposition delivers for the energy difference ΔE_c of a biaxial strained GeSn:

$$\Delta E_c = 0.136 \text{ eV} - 1.51y - 6.7 \text{ eps} \tag{2.24}$$

Crossover is obtained if Sn content y and biaxial strain eps fulfil the relation

$$1.51y + 6.7 \text{ eps} = 0.136 \text{ eV} \tag{2.25}$$

Applying strain changes the lattice cell volume. An increase is obtained with a tensile strain. The volume increase is much larger for biaxial strain than for uniaxial strain. The cubic cell is distorted to a tetragonal cell for a (100) substrate surface. The following relations for uniaxial and biaxial strains then give the cell volume changes.

Uniaxial strain: $\Delta V/V = \text{eps}*(1-2\,\nu) = \text{eps}*0.46$ (2.26)

Biaxial strain: $\Delta V/V = 2\text{eps}*[(1-2\,\nu)/(1-\nu)] = \text{eps}*1.26$ (2.27)

The Poisson number ν describes the contraction in a perpendicular direction to the tensile elastic stress; its value is 0.27 for Ge.

Comparison of Eqs. 2.26 and 2.27 proves that the volume change with biaxial strain is nearly three times higher than that with uniaxial

strain. Indeed, crossover with uniaxial strain requires more than 4% tension, in agreement with the simple volume considerations.

Both tensile biaxial strain and Sn alloying reduce the bandgap to about 0.5 eV for crossover.

A rough approximation for the direct bandgap E_{gdir} delivers as first overview

$$E_{\mathrm{gdir}} = 0.8\ \mathrm{eV} - 3.3\,y - 14.7\ \mathrm{eps} \tag{2.28}$$

This approximation is only valid for biaxial tensile strain. Strain splits the degenerate values of heavy holes and light holes. The lowest energy transition is related to the light hole valence band for biaxial tensile strain, whereas compressive biaxial strain moves up the heavy hole band. This causes a fundamental asymmetry of bandgaps concerning the sign of the strain (remark: tensile strain is counted positive, compressive strain negative).

References

1. Landolt-Börnstein (2001). *Group III-Condensed Matter*, Vol. 41, Semiconductors, electronically available at http://materials.springer.com.
2. C. F. Klingshirn (2012). *Semiconductor Optics*, 4th Ed. (Springer).
3. D. E. Aspnes and A. A. Studna (1983). *Phys. Rev. B*, **27**, 985.
4. E. Kasper and D. J. Paul (2005). *Silicon Quantum Integrated Circuits* (Springer).
5. J. Humlicek (2000). *Properties of Silicon Germanium and SiGe: Carbon, EMIS Datareviews Series*, Vol. 24 (INSPEC, IEE, London), p. 249.
6. M. Oehme, M. Kaschel, J. Werner, O. Kirfel, M. Schmid, B. Bahouchi, E. Kasper and J. Schulze (2010). Germanium on silicon photodetectors with broad spectral range, *J. Electrochem. Soc.*, **157**, 144–148.
7. J. Menendez, M. Noel, J. C. Zwickels and D. Lockwood (2017). Resonant indirect optical absorption in germanium, *Phys. Rev. B*, **96**, 121201.
8. J. Liu (2014). Monolithically integrated Ge-on-Si active photonics, *Photonics*, **1**, 162–197.
9. X. Wang and J. Liu (2018). Emerging technologies in Si active photonics, *J. Semicond.*, **39**, 061001, doi: 10.1088/1674-4926/39/6/061001.